MSDE

PAPER

View Article Online
View Journal | View Issue

Published on 05 January 2023. Downloaded by University of California - Los Angeles on 5/25/2023 8:37:38 AM.

Check for updates

Cite this: *Mol. Syst. Des. Eng.*, 2023, **8**, 611

Polyelectrolyte complex scaffoldings for photocrosslinked hydrogels†

Defu Li,[a] Mahsa Ghovvati,[a] Nasim Annabi [ab] and Samanvaya Srivastava *[acde]

Received 11th August 2022,
Accepted 5th January 2023

DOI: 10.1039/d2me00171c

rsc.li/molecular-engineering

Photocrosslinkable precursors (small molecules or polymers) undergo rapid crosslinking upon photoirradiation, forming covalently crosslinked hydrogels. The spatiotemporally controlled crosslinking, which can be achieved *in situ*, encourages the utility of photocrosslinked hydrogels in biomedicine as bioadhesives, bioprinting inks, and extracellular matrix mimics. However, the low viscosity of the precursor solutions results in unwanted flows and dilution, leading to handling difficulties and compromised strength of the photocrosslinked hydrogels. Here, we introduce oppositely charged triblock polyelectrolytes as additives for precursor solutions that transform them into self-assembled polyelectrolyte complex (PEC) hydrogels with enhanced shear strength and viscosity, providing interim protection against precursor dilution and mitigating secondary flows. The PEC network also augments the properties of the photocrosslinked hydrogels. Crosslinking of the precursors upon photoirradiation results in the formation of interpenetrating polymer network hydrogels with PEC and covalently-linked networks that exhibit shear moduli exceeding the linear combination of the moduli of the constituent networks and overcome the tensile strength–extensibility tradeoff that restricts the performance of covalently-linked hydrogels. The reinforcement approach is shown to be compatible with four types of photocrosslinkable precursors, does not require any modification of the precursors, and introduces minimal processing steps, paving the way for a broader translation of photocrosslinkable materials for biomedical applications.

Design, System, Application

Photocrosslinked hydrogels have attracted extensive research and clinical interest as bioadhesives, inks in extrusion-based 3D bioprinting, carriers for drug delivery, and scaffolding for tissue engineering. Although these hydrogels typically possess rigid structures after crosslinking, the low viscosity and shear strength of their precursors limit their application in situations involving uneven surfaces or excess fluids. We present self-assembled networks of oppositely charged block polyelectrolytes as scaffoldings to address these limitations and concomitantly enrich the microstructure and the mechanical properties of photocrosslinked hydrogels. We establish broad compatibility of our approach by demonstrating improvements in precursor and hydrogel properties for four distinct photocrosslinkable materials. Moreover, we present systematic approaches to enhance the viscosity and shear strength of the precursor solutions and the shear and tensile strength as well as the hierarchical microstructure of the photocrosslinked hydrogels by varying the concentration of and interactions between the block polyelectrolytes and photocrosslinkable precursors. We envision that the design rules for block polyelectrolyte reinforced photocrosslinkable precursors and hydrogels we present will facilitate their adoption in biomedicine.

Introduction

Photocrosslinked hydrogels are employed widely in biomedicine as bioadhesives,[1–6] inks for three-dimensional (3D) bioprinting,[7–20] carriers for drug delivery,[21–33] and scaffoldings for bone and cartilage tissue engineering.[7,21,22,34–45] Upon (ultraviolet) light activation, the photocrosslinkable precursors (small molecules or polymers) in aqueous solutions covalently crosslink to form three-dimensional water-laden networks.[7,22,34,46,47] Thus, precise spatiotemporal control of crosslink density, mechanical properties, and functionality is achieved by regulating light dosage.[21,47] The irreversible covalent linkages contribute to

[a] *Department of Chemical and Biomolecular Engineering, University of California, Los Angeles, Los Angeles, CA 90095, USA. E-mail: samsri@ucla.edu*
[b] *Department of Bioengineering, University of California, Los Angeles, Los Angeles, CA 90095, USA*
[c] *California NanoSystems Institute, University of California, Los Angeles, Los Angeles, CA 90095, USA*
[d] *Center for Biological Physics, University of California, Los Angeles, Los Angeles, CA 90095, USA*
[e] *Institute for Carbon Management, University of California, Los Angeles, Los Angeles, CA 90095, USA*

† Electronic supplementary information (ESI) available. See DOI: https://doi.org/10.1039/d2me00171c

Published on 05 January 2023. Downloaded by University of California - Los Angeles on 5/25/2023 8:37:38 AM.

their mechanical strength and structural stability in diverse environments regardless of pH and salt variations. In addition, the facile injectability of low-viscosity hydrogel precursor solutions into confined spaces makes them suitable for minimally invasive surgery applications.[34,47–49]

However, even with these desirable attributes and their use in myriad biomedical applications, photocrosslinked hydrogels still suffer from several shortcomings that limit their utility. Before light activation, the uncrosslinked precursor solutions typically have low viscosity and weak mechanical strength. When employed as bioadhesives, for instance, this results in unwanted secondary flows and a minimal capacity to conform to complex geometries of irregular, non-horizontal wound sites.[50] Moreover, wet environments created by blood and biological fluids at the wound site lead to dilution and deactivation of the precursors, resulting in potential adhesive failure.[50] Similar challenges emerge in extrusion-based 3D bioprinting applications, wherein the viscosity and the structural strength of the precursor solution are too poor to print a construct with adequate printing resolution, shape fidelity, and height.[51] Therefore, appropriate reinforcements of shear strength and viscosity of precursors are essential for expanding the utility of photocrosslinkable hydrogels.

Similarly, effective solutions to improve hydrogel's shear and tensile properties after photocrosslinking are highly anticipated. Typical covalently linked hydrogels (including photo-crosslinked hydrogels) suffer from a strength–extensibility tradeoff wherein their tensile strength, extensibility, and toughness cannot be all simultaneously enhanced by increasing polymer concentration.[52–56] Moreover, such hydrogels lack self-healing characteristics and stimuli responsiveness (pH and salt), owing to the *permanent* netpoints comprising the network.[57,58] Lastly, they possess simple microstructures, resulting in poor stress dissipation characteristics and an inability to encapsulate

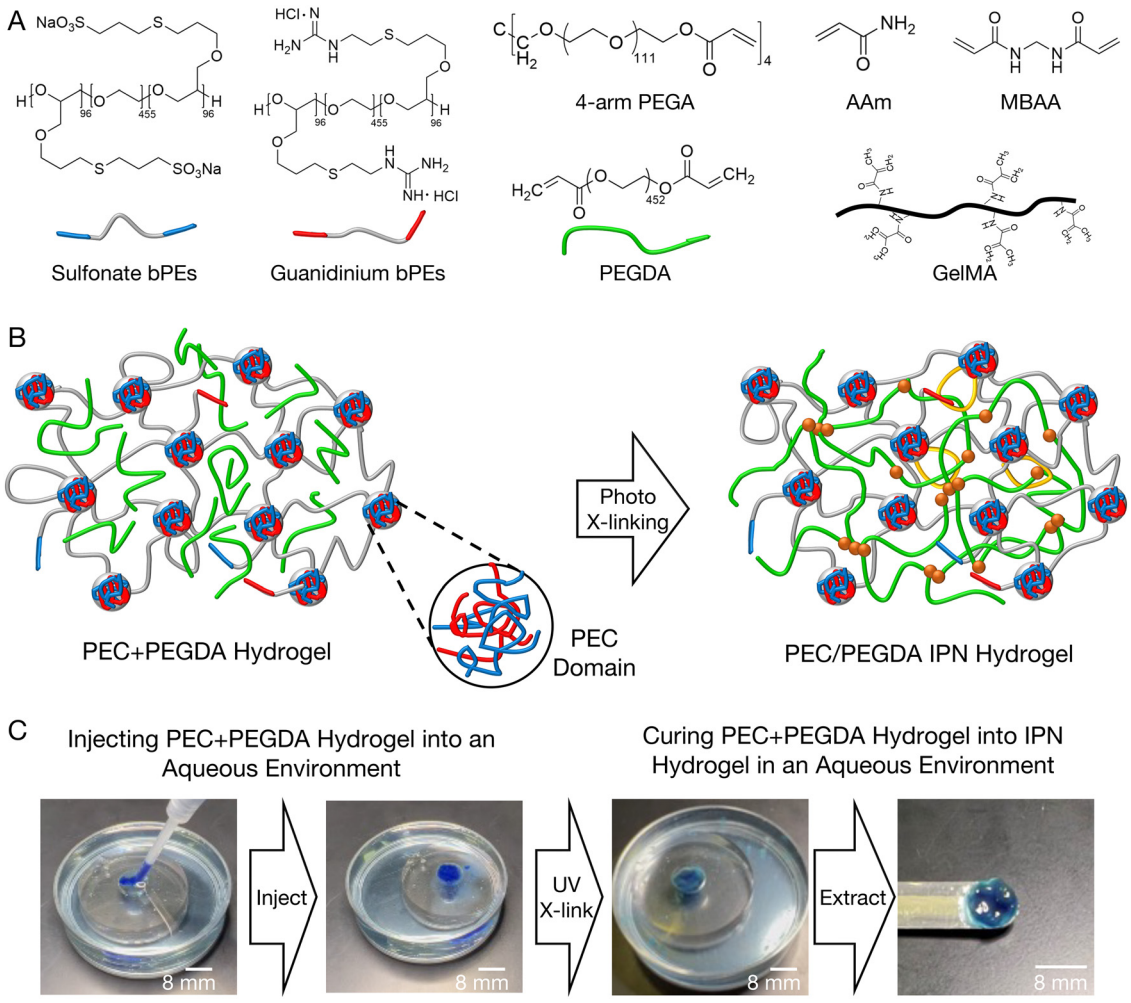

Fig. 1 PEC scaffoldings for photocrosslinked hydrogels. (A) Chemical structures of sulfonate functionalized bPEs, guanidinium functionalized bPEs, 4-arm poly(ethylene glycol)acrylate (4-arm PEGA), poly(ethylene glycol)diacrylate (PEGDA), acrylamide (AAm), *N*,*N*′-methylenebisacrylamide (MBAA), and gelatin methacryloyl (GelMA). (B) Schematic illustration of PEC + PEGDA hydrogels and PEC/PEGDA IPN hydrogels. (C) Photos demonstrating injectability and photocrosslinking of PEC + PEGDA hydrogels in an aqueous environment. Water and PEC + PEGDA hydrogels were both dyed with blue color to enhance visibility.

This journal is © The Royal Society of Chemistry and IChemE 2023

Published on 05 January 2023. Downloaded by University of California - Los Angeles on 5/25/2023 8:37:38 AM.

and release small molecule or macromolecule cargo (therapeutics, *etc.*).[59–61]

Here, we introduce a simple strategy to ameliorate the shortcomings of typical photocrosslinked hydrogels, both in the uncrosslinked and the crosslinked states, by harnessing polyelectrolyte complexation-driven self-assembly pathways. Oppositely charged triblock polyelectrolytes (bPEs), when introduced into the precursor solutions, self-assemble into 3D polyelectrolyte complex (PEC) networks swiftly, providing near-instant enhancements in viscosity and preventing dilution and flow of precursor solutions.[58,62–64] Photocrosslinking of the precursors containing PEC gels results in hydrogels with interpenetrating covalent and PEC networks exhibiting improved shear and tensile performance.[64] We demonstrate the generality of our approach by combining bPEs with four photocrosslinkable precursors, poly(ethylene glycol)diacrylate (PEGDA), 4-arm poly(ethylene glycol)acrylate (4-arm PEGA), acrylamide (AAm), and gelatin methacryloyl (GelMA), representing the diversity of precursor type (polymer *vs.* small molecule), structure (linear *vs.* star), and origin (synthetic *vs.* bioderived) (Fig. 1A). Starting with proof-of-concept demonstrations of the viability of our proposed approach, we discuss the improvements in shear properties of the uncrosslinked precursor solutions and shear and tensile properties of photocrosslinked hydrogels. Scattering measurements are employed to argue that these improvements emerge from the self-assembled PEC network that forms when bPEs are introduced in the precursor solutions and persists in the photocrosslinked hydrogels. We conclude by discussing the design principles for improved bPE-containing photocrosslinked hydrogels. We envision that the PEC hydrogel scaffoldings proposed here will facilitate a broader transition of existing photocrosslinkable materials from research products to clinical applications.

Materials and methods

Materials

Poly(ethylene oxide) (PEO, MW = 20 000 g mol^{-1}), potassium (99.5%), ally glycidyl ether (AGE), naphthalene, calcium hydride, *N*,*N*,*N*′,*N*′-tetramethylethylenediamine (TEMED), acrylamide, gelatin (from cold-water fish skin, MW ≈ 60 000 g mol^{-1}), triethylamine, acryloyl chloride, celite, methacrylic anhydride, 2,2-dimethoxy-2-phenylacetophenone (DMPA), sodium 3-mercapto-1-propanesulfonate (90%), *N*,*N*′-methylenebisacrylamide (MBAA), 1*H*-pyrazole-1-carboxamidine hydrochloride (99%), cysteamine hydrochloride (98%), and Irgacure 2959 were obtained from Sigma-Aldrich. 4-Arm poly(ethylene glycol) acrylate (MW = 20 000 g mol^{-1}) was obtained from JenKem Technology. All reagents were used as received.

Synthesis of triblock polyelectrolytes (bPEs)

Triblock polyelectrolytes (bPEs) were synthesized following previously published protocols.[58,62–64] PEO was dried under vacuum for 12 hours. AGE was dried by stirring with calcium hydride, degassed by three cycles of freeze-pump-thaw, and purified by distillation. 20 grams of PEO were dissolved in 60 mL anhydrous tetrahydrofuran (THF) at 40 °C in an Ar glove box. Potassium naphthalenide (0.4 M in THF) solution was then added to the PEO solution until the solution turned light green. Approximately 28 mL AGE was then transferred into the PEO solution, and the mixture was allowed to react for 48 hours at 40 °C. The product poly(ally glycidyl ether)$_{96}$-*b*-poly(ethylene oxide)$_{455}$-*b*-poly(ally glycidyl ether)$_{96}$ ($PAGE_{96}$-PEO_{455}-$PAGE_{96}$) was precipitated in hexane.

Thiol–ene click reactions were employed to functionalize the PAGE blocks with ionizable moieties. In a typical functionalization reaction, 2 g of $PAGE_{96}$–PEO_{455}–$PAGE_{96}$, cysteamine hydrochloride (5 equivalents per alkene), and DMPA (0.05 equivalents per alkene) were dissolved in a 30 mL equal volume water/DMF mixture.[58] The solution was degassed for 30 minutes by bubbling with N_2 and then exposed under UV light (365 nm, 8 watts) for at least 6 hours to produce ammonium-functionalized $PAGE_{96}$–PEO_{455}–$PAGE_{96}$. Sulfonate-functionalized $PAGE_{96}$–PEO_{455}–$PAGE_{96}$ was synthesized with the same procedure except for replacing cysteamine hydrochloride with sodium 3-mercapto-1-propanesulfonate. Guanidinium-functionalized $PAGE_{96}$–PEO_{455}–$PAGE_{96}$ was synthesized by dissolving 2 grams of ammonium-functionalized $PAGE_{96}$–PEO_{455}–$PAGE_{96}$ and 1*H*-pyrazole-1-1-carboxamidine hydrochloride (5 equivalent per amine) in 200 mL phosphate-buffered saline (PBS) buffer. The pH of the solution was adjusted to 10 and the reaction mixture was stirred at room temperature for 3 days. All reaction mixtures were dialyzed against deionized water for 10 cycles of 12 hours each using regenerated-cellulose dialysis tubing (MWCO 3.5 K, Fisher Scientific) to remove excess reagents and lyophilized to collect dry final products, which were characterized by ^{1}H NMR (Fig. S1†).

Synthesis of gelatin methacryloyl (GelMA)

Gelatin was dissolved in Dulbecco's phosphate-buffered saline (DPBS) (HyClone) to prepare 10% (w/v) solution, to which 8% (v/v) methacrylic anhydride was added dropwise under stirring.[65] The reaction was performed at around 60 °C and terminated after 2.5–3 hours by 2–3 fold dilution with preheated DPBS (~60 °C). The reaction mixture was dialyzed against deionized water in dialysis tubes (Spectrum Laboratories, MWCO 12–14 kDa) for 14 cycles of 12 hours each to remove unreacted reactants and solvents.[65] The purified solution was lyophilized to collect a white spongy final product, which was characterized by ^{1}H NMR (Fig. S2A†).

Synthesis of poly(ethylene glycol)dimethacrylate (PEGDA)

30 grams of PEG was dissolved in 160 mL of anhydrous toluene under stirring. The solution was heated to 125 °C to distill out approximately 40 mL of toluene to remove any trace amount of water,[66] cooled to 40 °C and sparged with N_2 gas. Triethylamine (8 equivalents per PEG chain) was added

Published on 05 January 2023. Downloaded by University of California - Los Angeles on 5/25/2023 8:37:38 AM.

to the solution.[67] After 10 minutes, acryloyl chloride (8 equivalents per PEG chain, diluted with 10 mL anhydrous toluene) was added dropwise into the solution. After 90 minutes, the product solution was filtered twice through fritted funnel filled with Celite®545.[66] The product solution was precipitated in 4 °C hexane, dried under vacuum, and characterized by ^{1}H NMR (Fig. S2B†).

Hydrogel preparation

PEC hydrogels were prepared by mixing aqueous solutions of oppositely charged bPEs with a molar charge ratio of 1 : 1 in deionized water. PEC + precursor hydrogels were prepared by mixing sulfonate functionalized bPEs with the precursor and 0.5 wt% photoinitiator 2959 in deionized water, followed by the addition of an aqueous solution of guanidinium functionalized bPEs. The mixtures were mixed on a vortex mixer for 60 seconds to obtain homogenous hydrogels. The PEC + precursor hydrogels were placed in polydimethylsiloxane (PDMS) molds and irradiated with ultraviolet (UV) light (302 nm, 8 W) for 10 minutes to obtain the corresponding PEC/covalent hydrogels. The PEC/AAm IPN hydrogels required an additional MBAA crosslinker, added at a molar ratio of AAm : MBAA = 1 : 54, TEMED catalyst (0.5 wt%), and 30 minutes of UV light exposure to form the polyacrylamide network. A 0.16 mm thick micro cover glass (VWR) was placed on the top of PDMS molds to minimize water evaporation during UV irradiation.

Rheology

Rheology measurements with steady and oscillatory strains were carried out on an Anton Paar MCR 302 rheometer. The viscosity of precursor solutions as a function of shear rate were measured by using a cone and plate fixture (diameter: 50 mm, core angle: 1°). The precursor solutions were placed on the bottom plate and trimmed before initiating the measurements. The shear moduli were measured using a parallel plate (diameter: 8 mm, gap height: 0.7 mm) for covalent or IPN hydrogels and a cone and plate fixture (diameter: 10 mm, cone angle: 2°) for PEC or PEC + precursor hydrogels. The PEC or PEC + precursor hydrogel samples were placed on the bottom plate and trimmed before initiating the measurements. Covalent or IPN hydrogels were prepared for rheology measurements by placing 70 μL of precursor solution or PEC + precursor hydrogels solution using a positive displacement pipet into a cylindrical PDMS mold (diameter 8 mm, height 1.5 mm) and photocrosslinked by UV irradiation. The crosslinked samples were placed in between the parallel plates of the measurements fixture. Water evaporation was minimized during testing by using a solvent trap. All samples were pre-sheared for 195 s at strain γ = 0.8% and frequency ω = 1 rad s^{-1} to achieve a stabilization of the shear moduli. Amplitude sweeps with γ ranging from 0.01% to 100% at ω = 1 rad s^{-1} were employed to determine the linear viscoelastic regime (Fig. S3†). Frequency sweeps were carried out with ω ranging from 0.1 to 20 rad s^{-1} and γ = 0.8% (within the LVE region). All measurements were carried out at 25 °C.

Tensile testing

Tensile measurements were performed by employing an Instron 5943 tensile system. 120 μL of precursor solutions or PEC + precursor hydrogels were placed into a cuboid PDMS mold (length: 18 mm, height: 4.5 mm, width: 1.5 mm), followed by UV irradiation. The two ends of crosslinked hydrogel samples were affixed on two pieces of rigid plastic film (ARcare 90445Q) using super glue. The plastic films were mounted on the machine tension grips. The uniaxial stretch rate was set to 6 mm min^{-1} to stretch the hydrogel samples until the hydrogel ruptured. The ultimate stress was collected by locating the maximum stress that a tensile sample could withstand before rupture, and the corresponding strain was defined as extensibility. Young's modulus was calculated by the slope of stress–strain curves in the linear elastic region. Toughness, quantifying the ability of hydrogels to absorb energy before fracture, was determined by integrating the area under a stress *vs.* unitless strain curve. The statistical analysis was performed by ANOVA two-way without replication (alpha value = 0.05, MS Excel). All data of ultimate strength, extensibility, Young's modulus, and toughness are reported as mean ± standard deviation.

Small-angle X-ray scattering (SAXS)

SAXS characterizations were performed at beamline 12-ID-B at Advanced Photon Source, Argonne National Laboratory. The sample-to-detector distance was set at 2.0 m, enabling SAXS spectra collection over scattering wave vector q ranging from 0.004 Å^{-1} to 0.8 Å^{-1}. Hydrogel samples were loaded into the gel sample holders and sealed with Kapton tape to minimize water evaporation and exposed to X-rays for 0.1 s at room temperature. One-dimensional SAXS spectra were obtained from two-dimensional scattering data by the matSAXS package. SAXS spectra from the hydrogels were obtained by subtracting the background spectra from the raw spectra obtained from the hydrogels using the Irena package in Igor Pro.

Results and discussion

PEC hydrogels self-assemble nearly instantly upon mixing aqueous solutions of the oppositely charged bPEs. The hydrogelation is driven by electrostatic interactions between the oppositely charged bPEs and the entropy gains from counterion release, resulting in their associative phase separation.[68–70] The neutral middle blocks of the bPEs, however, restrict macroscale phase separation, resulting in the formation of a three-dimensional, physically crosslinked polymer network comprising nanoscale polymer-rich PEC domains (composed of the oppositely charged end-blocks) interconnected *via* the neutral blocks.[62] These PEC hydrogels are injectable, extrudable, and maintain interim resistance against dissolution and swelling upon injection in water, even upon shaking (Fig. S4 and Movie SM1†).

 This journal is © The Royal Society of Chemistry and IChemE 2023

Published on 05 January 2023. Downloaded by University of California - Los Angeles on 5/25/2023 8:37:38 AM.

PEC hydrogels serve as supportive matrices for photocrosslinkable precursors enabling their application and curing in aqueous surroundings by offering protection against dilution, materials loss, and deactivation. To ensure adequate mixing, the precursors were mixed with the negatively charged bPEs, followed by the addition of the positively charged bPEs. Charge-driven self-assembly of the bPEs resulted in PEC hydrogels with homogeneously distributed precursor materials, denoted as PEC + precursor hydrogels (Fig. 1B shows a representative schematic of PEC + PEGDA hydrogel). When injected onto underwater glass substrates, the PEC + precursor hydrogels conserve the precursors in aqueous surroundings without any apparent dilution (Fig. 1C; see also Fig. S5–S8 and Movies SM2–SM5†). The PEC hydrogel scaffolding retained the precursor materials, providing sufficient time for photocrosslinking of the precursors. Upon UV irradiation, crosslinking of the precursor formed a covalent network, transforming the PEC + precursor hydrogels into PEC/covalent interpenetrating polymer network (IPN) hydrogels (Fig. 1C). In contrast, dilution of uncrosslinked precursors occurred immediately when exposed to aqueous media, making them incapable of forming crosslinked hydrogels (Fig. S9–S12 and Movies SM6–SM9†). We note that no modification of the precursors was required to make them amenable to our reinforcement strategy; they were mixed as received or synthesized with the bPEs to create the PEC + precursor hydrogels.

Modulating the viscosity and shear response of photocrosslinkable precursors

PEC hydrogels serve as a scaffolding supporting photocrosslinkable precursors by forming a precursor-encapsulating hydrogel. These PEC + precursor hydrogels possess viscoelastic attributes that are significant improvements over the corresponding properties of the precursor solutions. For instance, the viscosity of 15 wt% solutions of PEGDA, 4-arm PEGA, and GelMA are all ~0.01 Pa s, and of 15 wt% solution of AAm was even lower (~0.001 Pa s), similar to water (Fig. 2A). Incorporation of 30 wt% bPEs enhanced the viscosity of resultant PEC + precursor hydrogels by three to five orders of magnitude (Fig. 2A), enabling easier handling of precursors.

PEC networks also imbue shear strength to resulting PEC + precursor hydrogels. Varying the content of the precursors (C_{PC}) and the bPEs (C_{bPE}) allowed for facile tuning of the shear properties of the PEC + precursor hydrogels. Fig. 2B–E highlights the tunability of the shear moduli of PEC + precursor hydrogels, depicting the evolution of storage (G') and loss (G'') moduli of PEC + precursor hydrogels with increasing C_{bPE} (at constant C_{PC}) (Fig. 2B and C) and with increasing C_{PC} (at constant C_{bPE}) (Fig. 2D and E). Increasing C_{bPE} from 10 to 40 wt% while keeping C_{PC} = 5 wt% improved both G' and G'' of PEC + precursor hydrogels progressively (Fig. 2B and C, see also Fig. S13 and S14†), ascribable to the concomitantly increasing density of the PEC domains and shear strength of the PEC network. At the same time, increasing C_{PC} from 5 to 20 wt% while maintaining a constant C_{bPE} = 30 wt% led to a progressive lowering of the shear moduli of the resulting PEC + precursor hydrogels (Fig. 2D and E, see also Fig. S15 and S16†). We posit that the photocrosslinkable precursors encapsulated within the PEC network crowd the interstitial spaces between the PEC domains. This resulted in steric hindering of the bridging among the PEC domains by the neutral midblocks and promoting loop formation, reduced the PEC network

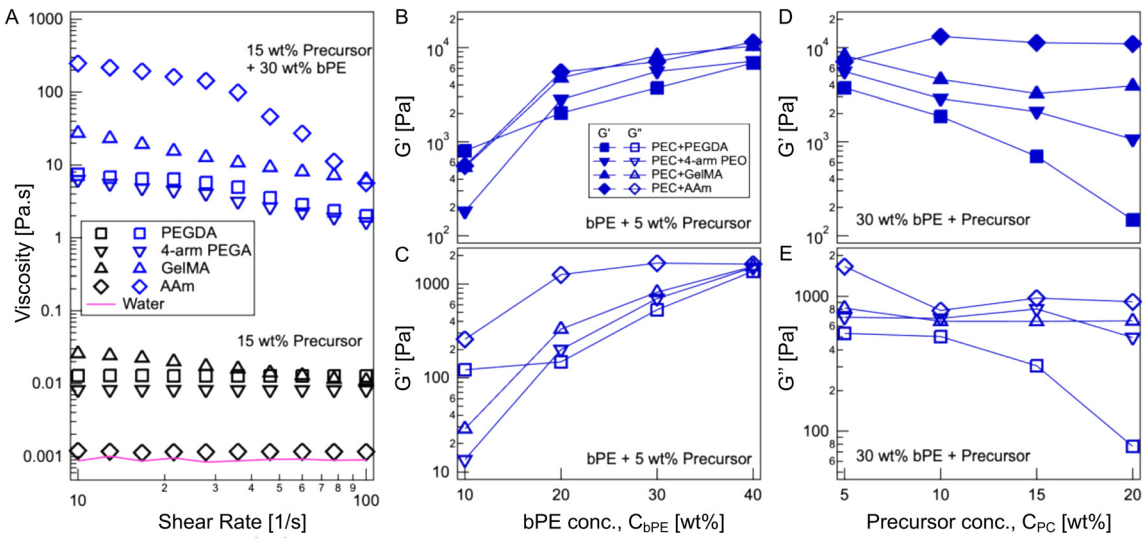

Fig. 2 Enhancing shear properties of precursor solution with PEC hydrogel scaffoldings. (A) Viscosity of precursor solutions and PEC + precursor hydrogels *versus* shear rate profiles demonstrating that incorporation of bPEs in precursor solutions enhanced their viscosity significantly. Data shown for 15 wt% precursor solutions (black symbols) and PEC + precursor hydrogels (blue symbols) with 30 wt% bPEs and 15 wt% precursors. (B and D) Storage (G') and (C and E) loss (G'') moduli of PEC + precursor hydrogels with a constant C_{PC} = 5 wt% and varying C_{bPE} (B and C), and with a constant C_{bPE} = 30 wt% and varying C_{PC} (D and E).

Published on 05 January 2023. Downloaded by University of California - Los Angeles on 5/25/2023 8:37:38 AM.

connectivity, and thus reduced the shear moduli of the PEC + precursor hydrogels.[64] This steric hindrance by the precursors and the accompanying reduction in moduli with increasing C_{PC} is expected to be dictated by the size of the precursor molecules (PEGDA > 4-arm PEGA > AAm) and thus is most prominent for PEC + PEGDA hydrogels, followed by PEC + 4-arm PEGA hydrogels, and least prominent for PEC + AAm hydrogels (Fig. 2D and E). Interactions of the precursors with the charged blocks of the bPEs are also expected to influence PEC network formation and the shear moduli of the resulting hydrogels. For example, GelMA chains comprise charged functional groups (*e.g.*, guanidinium and carboxylic acid groups)[71,72] which could interact with the sulfonate and the guanidinium moieties on the bPEs, respectively, and influence PEC network connectivity and shear moduli. Both these factors can be combined to precisely tune the viscoelastic behavior of the PEC + precursor hydrogels to meet the varying requirements of diverse biomedical applications requiring *in situ* polymerization, such as extrusion-based 3D bioprinting and bioadhesion.

Enhancing the shear strength of photocrosslinked hydrogels

The PEC network not only serves as a scaffolding for the crosslinkable precursors but also enhances the shear moduli of the crosslinked hydrogels. Upon photoirradiation, the precursors encapsulated in the PEC + precursor hydrogels crosslinked to form covalent networks, which interpenetrated with PEC networks to form IPN hydrogels. The interpenetration of the two networks is evident from the marked improvements in shear strengths of the IPN hydrogels compared to the corresponding PEC hydrogels or covalently crosslinked hydrogels. Fig. 3 shows the frequency (ω) dependence of G' and G'', subjected to oscillatory shear strain with γ = 0.8%, for PEC hydrogels (grey circles), covalent hydrogels (black symbols), and the corresponding IPN hydrogels (red symbols) comprising C_{PC} = 15 wt% and C_{bPE} = 30 wt% (see also Fig. S17 and S18†). All the hydrogels exhibit ω-independent moduli indicating robust PEC, covalent, and interpenetrating PEC/covalent networks. Notably, the shear moduli of the IPN hydrogels were higher than those of either of the constituent networks across the investigated ω range.

Fig. 4 shows the comparison of G' and G'' (measured at ω = 1.12 rad s^{-1} and γ = 0.8%) for PEC hydrogels (grey circles), covalently crosslinked hydrogels (black squares), and the corresponding IPN hydrogels (red circles) comprising C_{PC} varying between 5 and 20 wt% and a constant C_{bPE} = 30 wt%. We note that all the PEC, covalent, and IPN hydrogels, except the 5 wt% covalent hydrogels, exhibited ω-independent moduli (Fig. S14, S17, and S18†). The trend of IPN hydrogels possessing higher shear moduli than either the PEC network or the covalently crosslinked network persisted across the range of C_{PC}; for all the four kinds of photocrosslinked networks investigated here. Upon increasing C_{PC}, the moduli of the photocrosslinked hydrogels increased owing to denser covalent networks (Fig. S17†). Similarly, increasing C_{PC} continually strengthened the shear moduli of the IPN hydrogels.

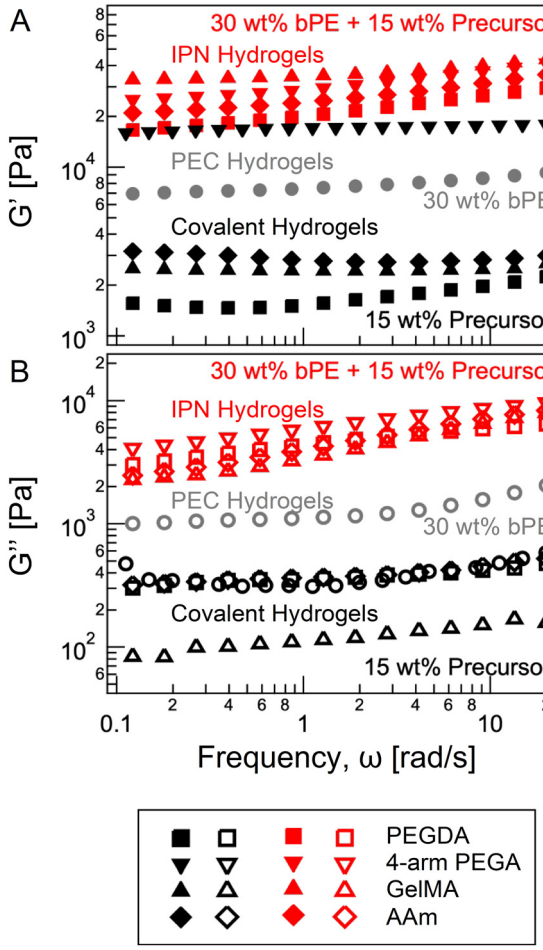

Fig. 3 Frequency response of covalent, PEC, and IPN hydrogels. (A) Storage (G') and (B) loss (G'') moduli of PEC (grey symbols), covalent (black symbols), and IPN (red symbols) hydrogels as a function of frequency (ω) of oscillatory strain with strain amplitude γ = 0.8%.

It is plausible that the crosslinking of the photocrosslinkable precursors is hindered when pursued amidst the PEC network, owing to reduced mobility of the precursors, steric hindrance by the PEC network, and the higher optical density of the PEC + precursor hydrogels as compared to the nearly transparent aqueous precursor solutions. This would imply a lower moduli contribution from partially crosslinked covalent networks to the moduli of the IPN hydrogels. At the same time, entanglements between the PEC and the covalent networks are expected to contribute to the shear strength of the IPN hydrogels. Notably, the shear moduli of all the IPN hydrogels considered here (red circles in Fig. 4) were larger than the sum of the shear moduli of individual covalent hydrogels and PEC hydrogels (purple diamonds in Fig. 4). Thus, it can be argued that the excess entanglements emerging from the interpenetration of the two networks not only compensate for the loss of the shear strength caused by deficiencies in the crosslinking of the covalent network but also contribute an excess shear strength

This journal is © The Royal Society of Chemistry and IChemE 2023

Published on 05 January 2023. Downloaded by University of California - Los Angeles on 5/25/2023 8:37:38 AM.

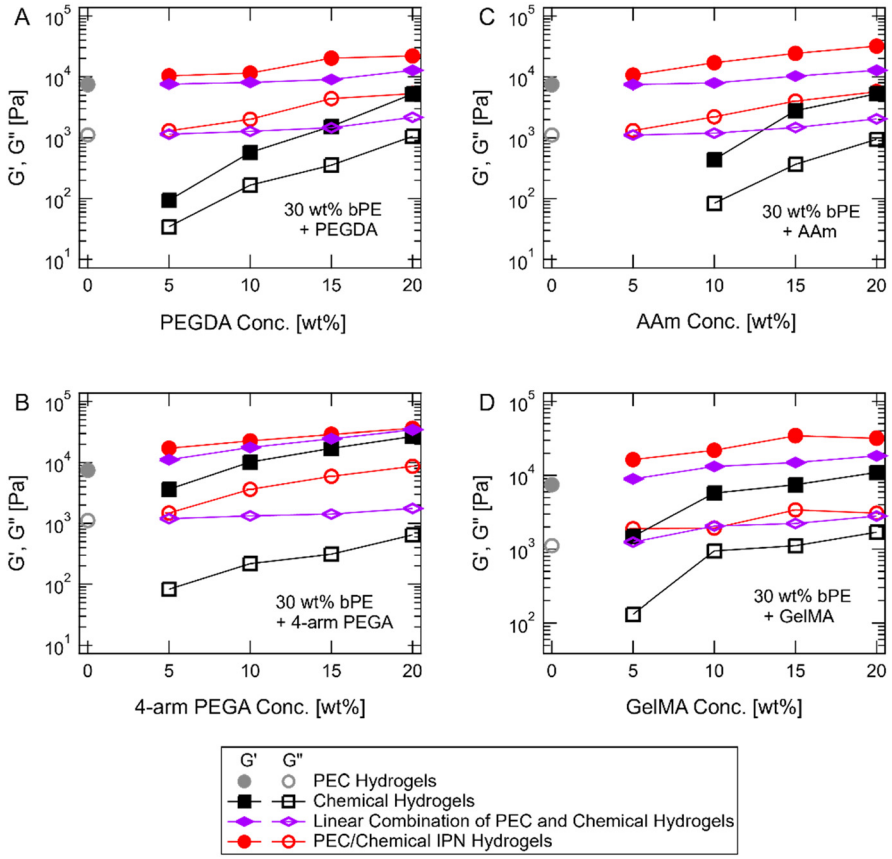

Fig. 4 Shear moduli tunability and synergistic effects in IPN hydrogels. Storage moduli (G') and loss moduli (G'') of covalent (black squares) and PEC/covalent IPN hydrogels (comprising 30 wt% bPEs, red circles), measured at ω = 1.12 rad s^{-1} and γ = 0.8%, as a function of precursor concentration C_{PC}. The shear moduli of the corresponding 30 wt% PEC hydrogels are also shown with grey circles. Purple diamonds depict the linear combination of the moduli of PEC and covalent hydrogels. (A) PEGDA-based hydrogels, (B) 4-arm PEGA-based hydrogels, (C) AAm-based hydrogels, and (D) GelMA-based hydrogels.

than those achievable by a linear combination of the strengths of the constituent networks.

The hindrance of crosslinking is expected to be proportional to the mobility limitations that the precursor molecules encounter in the PEC network, which in turn is expected to be inversely proportional to the size of the precursor molecules. Thus, small AAm molecules are expected to form a robust network in the presence of the PEC network, while the long PEGDA chains are expected to face the most significant hindrance. 4-Arm PEGA chains should face similar transport limitations as the PEGA chains, with faster transport owing to their slightly smaller size offset by the participation of each chain in twice the number of crosslinks. Concomitantly, the moduli enhancements are the largest for PEC/AAm IPN hydrogels, followed by comparable enhancements for PEC/PEGDA IPN hydrogels and PEC/4-arm PEGA IPN hydrogels (see Fig. S15, S16, and S18†). In addition, covalent networks carrying functional groups that interact with the charge-bearing moieties on the bPEs can contribute further enhancements to the IPN hydrogel moduli. For example, PEC/GelMA IPN hydrogels exhibited larger improvement in G' compared with IPN hydrogels comprising neutral covalent chains, attributable to the interactions between the guanidinium and carboxylic acid groups on the GelMA network and the sulfonate and the guanidinium moieties on the bPEs, contributing another mechanism for stress dissipation.

Enhancing the tensile properties of photocrosslinked hydrogels

The ultimate tensile strength and the Young's modulus of chemically crosslinked hydrogels can be typically enhanced by increasing the precursor concentrations. However, such enhancements are usually accompanied by a loss of extensibility due to a higher crosslinking density and denser covalent networks. Thus, improving the toughness of such hydrogels becomes particularly challenging owing to this strength–extensibility tradeoff.[52–56]

Reinforcement of the covalent networks with the PEC networks mitigated the tensile strength–extensibility tradeoff by enabling independent modulation of strength and extensibility of the resulting IPN hydrogels (Fig. 5). Moreover, the linear elastic response of the photocrosslinked hydrogels transitioned to a markedly non-linear response upon the introduction of the PEC networks (representative stress–

Published on 05 January 2023. Downloaded by University of California - Los Angeles on 5/25/2023 8:37:38 AM.

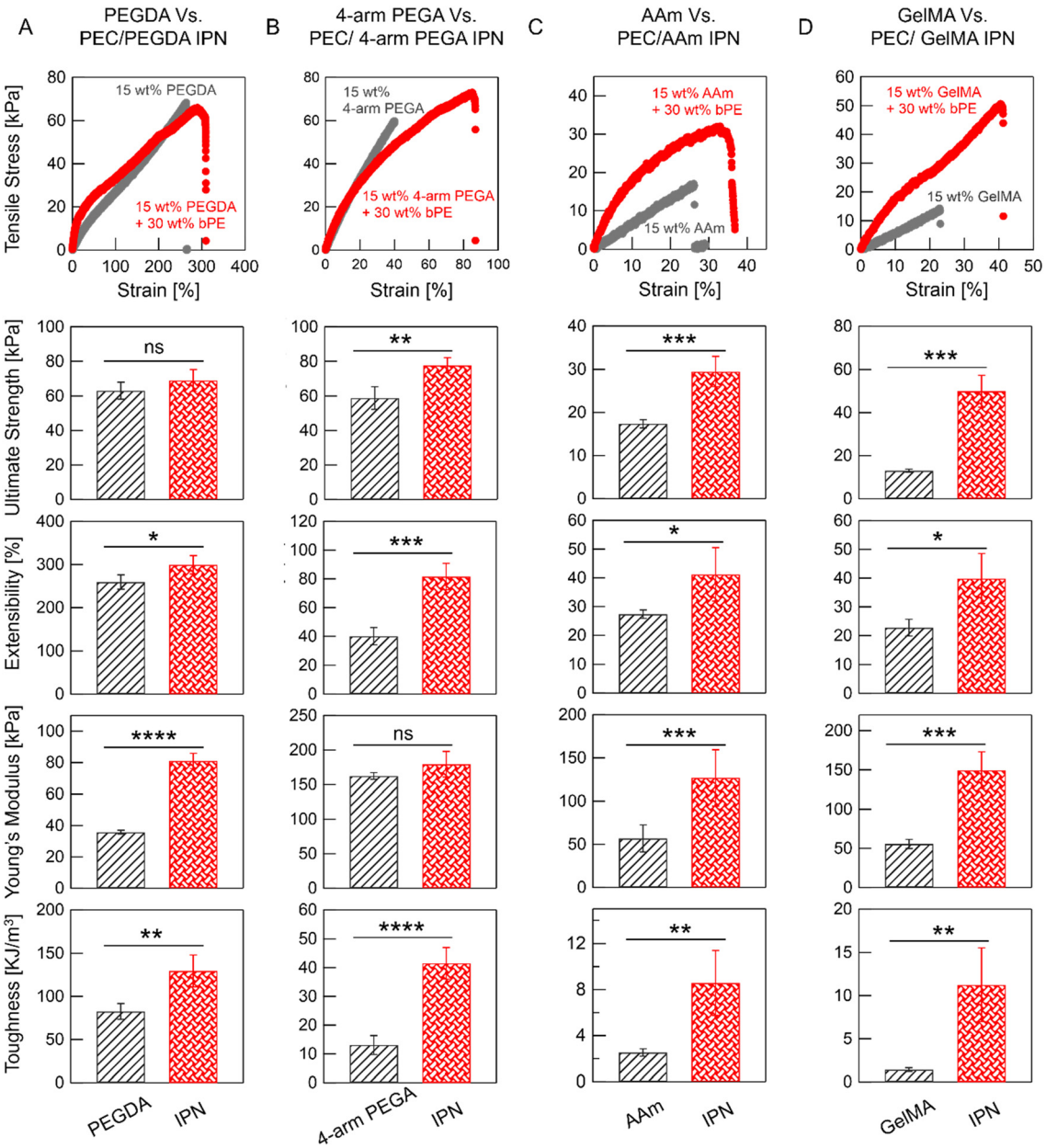

Fig. 5 Comparing the tensile properties of covalent and IPN hydrogels. Representative tensile stress–strain curves, ultimate strength, extensibility, Young's modulus, and toughness of covalent hydrogels (grey data) and PEC/covalent IPN hydrogels (red data), with C_{PC} = 15 wt% and C_{bPE} = 30 wt%. (A) PEGDA-based hydrogels (B) 4-arm PEGA-based hydrogels, (C) AAm-based hydrogels, (D) GelMA-based hydrogels. Samples tested ≥4. The data are shown as mean ± standard deviation (not significant (ns): $p > 0.1$, *: $0.1 > p > 0.05$, **: $0.05 > p > 0.01$, ***: $0.01 > p > 0.001$, ****: $0.001 > p$).

strain curves are shown in Fig. 5, row 1, see also Fig. S19 and S20†). The tensile properties of the covalent and the IPN hydrogels with C_{PC} = 15 wt% and C_{bPE} = 30 wt%, as extracted from the uniaxial tensile testing, are shown in Fig. 5, rows 2–5. In general, improvements in ultimate strength, extensibility, Young's moduli, and toughness were noted upon introducing the PEC networks. However, the magnitude of the improvements depended on the molecular structure of the precursors and their interactions with the bPE chains.

The tensile strength of the IPN hydrogels is expected to have contributions from the stress–bearing covalent networks, the stress-dissipative PEC networks, and the entanglements between the two interpenetrated networks. Expectedly, enhancements in tensile strength in the IPN hydrogels over the covalent hydrogels were observed (-Fig. 5, row 2). Commensurate with the trends in the shear strength, PEC/AAm IPN hydrogels and PEC/GelMA IPN hydrogels exhibited notable improvements in the tensile strength, ascribable to the robustness of the AAm network and the favorable interactions between GelMA and bPE chains, respectively. At the same time, PEC/PEGDA and PEC/4-arm PEGA IPN hydrogels experienced hindrances in

 This journal is © The Royal Society of Chemistry and IChemE 2023

Published on 05 January 2023. Downloaded by University of California - Los Angeles on 5/25/2023 8:37:38 AM.

covalent crosslinking and smaller enhancements in the tensile strengths.

Enhancements in extensibility were also noted in the IPN hydrogels as compared to the corresponding covalent hydrogels (Fig. 5, row 3). The extensibility of the IPN hydrogels is expected to be dictated by the crosslink density of the covalent network, with the additional entanglements contributed by PEC network contributing to inhibit chain relaxation and reducing the extensibility. Thus, the observed enhancements indicated a lower crosslinking density of covalent networks caused by topological constraints introduced by the PEC network. These enhancements were subtle in IPN hydrogels comprising PEGDA or AAm, while marked in IPN hydrogels comprising 4-arm PEGA or GelMA networks, commensurate with the stronger constraints that the 4-arm PEGA or the GelMA chains faced, owing to a high crosslink density or additional constraints owing to electrostatic interactions with the bPEs, respectively.

Entanglements between the interpenetrating networks also improved the Young's modulus of the IPN hydrogels owing to their contributions to the initial resistance to deformation (Fig. 5, row 4). In covalent hydrogels, the crosslinking density dictates the Young's modulus – the Young's modulus of 4-arm PEGA hydrogels was three-fold higher than that of PEGDA hydrogels. The polymer entanglements serve as additional crosslinks, resulting in notable improvement in Young's modulus of IPN hydrogels comprising PEGDA or AAm networks; the electrostatic interactions between the GelMA and bPE chains further enhance the modulus of the PEC/GelMA IPN hydrogels. The PEC/4-arm PEGA IPN hydrogels only had a subtle improvement in Young's modulus, which can again be attributed to the incomplete crosslinking of the 4-arm PEGA networks in the IPN hydrogels.

Enhancements in both ultimate strength and extensibility in IPN hydrogels led to their higher toughness. As shown in Fig. 5, row 5, IPN hydrogels comprising non-interacting covalent and bPE networks experienced two- to four-fold improvement in toughness compared to covalent hydrogels. The toughness of PEC/GelMA IPN hydrogel increased by nearly eight-fold, attributable to the toughening contributed by the reversible electrostatic interactions between the bPE and GelMA chains. Thus, by selecting appropriate photocrosslinkable precursors, IPN hydrogels with targeted tensile properties can be fabricated.

Imbuing hierarchical microstructure to photocrosslinked hydrogels

The scaffolding and the enhancements provided to the photocrosslinkable precursors and the crosslinked hydrogels, respectively, emerge from the PEC network that forms upon the mixing of the oppositely charged bPEs. This self-assembly of bPEs results in the formation of PEC domains comprising the oppositely charged blocks of the bPEs and interconnected by the neutral blocks. We argue that this self-assembled network also imbues a hierarchical microstructure to the IPN hydrogels, which is a distinct improvement over the simple network of photocrosslinked chains.

Small-angle X-ray scattering (SAXS) measurements provided further insights into the structure of the PEC network, specifically the size and structural arrangement of PEC domains and the average distance between them, and how they evolve upon interpenetration with the covalent networks. Fig. 6A shows representative SAXS spectra from PEC hydrogels with C_{bPE} = 30 wt% (grey trace), PEC + precursor hydrogels with C_{bPE} = 30 wt% and C_{PC} = 15 wt% (blue traces), and the corresponding IPN hydrogels (red traces). The broad primary (near q = 0.0201 Å^{-1}) in the SAXS spectra of 30 wt% PEC hydrogels indicated a disordered sphere microstructure of PEC domains. Upon the introduction of the photocrosslinkable precursors, the primary peak sharpened, transforming into a Bragg reflection peak and accompanied by the emergence of secondary peaks. These sharp peaks persisted upon crosslinking of the precursors and formation of the IPN hydrogels. The relative positioning of the primary and secondary peaks revealed parallelly stacked lamellar morphology of the PEC domains in the PEC + precursor hydrogels and the IPN hydrogels with C_{bPE} = 30 wt% and C_{PC} = 15 wt%, except for PEC + AAm hydrogels which featured hexagonally close-packed arrangements of cylindrical PEC domains.

Tunability in the PEC network microstructure (PEC domain morphology and arrangements) was achieved by varying the bPE and the precursor concentrations. As illustrated in Fig. 6B and C, increasing C_{PC} induced morphological evolution accompanied by an ordering transition, depending on the precursor type. Initially, a disordered arrangement of spherical PEC domains was observed in PEC hydrogels across C_{bPE} ranging from 10 to 40 wt% (Fig. S21–S23†). The incorporation of precursors, up to C_{PC} = 10 wt% in C_{bPE} = 10 wt% PEC hydrogels (Fig. 6B, see also Fig. S24†) or up to C_{PC} = 5 wt% in C_{bPE} = 30 wt% PEC hydrogels (Fig. 6C, see also Fig. S25†), and their subsequent crosslinking preserved the PEC domain morphology (yellow shaded region in Fig. 6B and C). At higher C_{PC}, a transition to parallelly-stacked lamellar morphology was observed in nearly all PEC + precursor and IPN hydrogels (green shaded region in Fig. 6B and C), with a few exceptions as discussed below.

The morphological and ordering transitions are hypothesized to emerge from the macromolecular crowding contributed by the precursor molecules between the PEC domains, increasing the effective volume fraction of the bPE chains. Similar transitions have been reported earlier in PEC hydrogels with increasing bPE concentration[63,64] or upon inclusion of polymeric additives.[64] The microstructure of the ordered PEC + precursor hydrogels or PEC/covalent hydrogels can be envisaged to comprise microcrystalline "grains" of ordered PEC domains with the precursor molecules or the covalent network residing in the interstitial spaces between the PEC domains, including the grain boundaries. We note

Published on 05 January 2023. Downloaded by University of California - Los Angeles on 5/25/2023 8:37:38 AM.

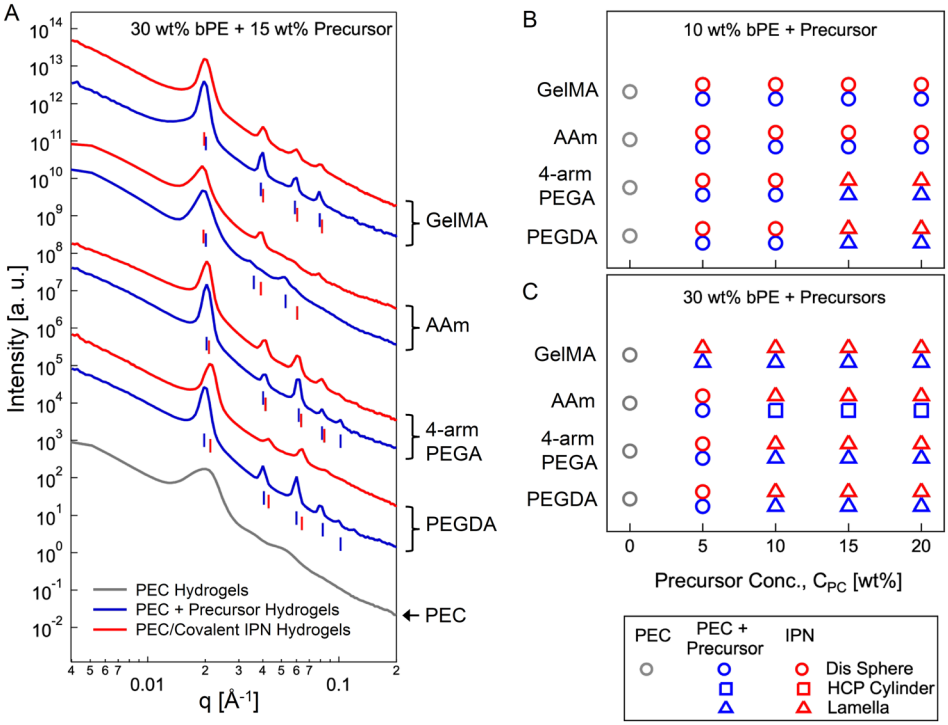

Fig. 6 Microstructural evolution of PEC, PEC + precursor, and IPN hydrogels. (A) Representative one-dimensional small-angle X-ray scattering spectra from PEC hydrogels (grey) with C_{bPE} = 30 wt%, and the PEC + precursor (blue) and PEC/covalent IPN (red) hydrogels with C_{bPE} = 30 wt% and C_{PC} = 15 wt%. Spectra from hydrogels comprising PEGDA, 4-arm PEGA, AAm, and GelMA-based are shown from bottom to top. The spectra are shifted vertically for clarity. The vertical bars denote the positions of primary and secondary Bragg peaks. Bragg peak locations are summarized in Tables S1–S6.† (B and C) The microstructural evolution of PEC, PEC + precursor, and IPN hydrogels with (B) C_{bPE} = 10 wt% and (C) C_{bPE} = 30 wt% as a function of C_{PC}. The symbols represent the following: circles – disordered spheres; squares – hexagonally packed cylinders; and triangles – lamellae.

that these microcrystalline grains are expected to be small, and we do not expect any macrophase separation of the PEC network and the precursor chains or the covalent network, as the Bragg peaks observed in the SAXS spectra are relatively short and broad, and the interdomains distances (estimated from the inverse of the position of the primary peak in the scattering spectra) remain nearly constant upon the progressive introduction of the precursors (see Fig. S26 and S27†). The SAXS spectra were generally location-independent, indicating the similarity of the microstructure of the PEC + precursor and PEC/covalent IPN hydrogels, at least at the scale of the size of the X-ray beam (50 μm × 200 μm). Lastly, a robust enhancement in the shear and tensile properties of the IPN hydrogels further support the hypothesis that the two networks do not macrophase separate.

With increasing size of the precursor molecules (AAm < 4-arm PEGA < PEGDA), the crowding is expected to be more significant, resulting in morphological transitions at smaller C_{PC} values. This trend is illustrated in Fig. 6B, wherein morphological transitions of the PEC domains are observed only in 4-arm PEGA or PEGDA containing PEC hydrogels or IPN hydrogels, but not in AAm containing hydrogels. Moreover, as shown in Fig. 6C, the PEC domains transform from spheres into cylinders upon incorporation of >10 wt% AAm monomers followed by a transition into lamellae upon photocrosslinking, commensurate with the enhanced crowding effects upon AAm network formation (blue shaded region in Fig. 6C). At the same time, the evolution of PEC network microstructure is further convoluted by the interactions between GelMA and bPE chains. At low C_{bPE}, GelMA did not have any effect on the PEC domain morphology (Fig. 6B). However, at higher C_{bPE} (≥ 30 wt%, Fig. 6C, see also Fig. S21†), introduction of even 5 wt% of GelMA induced a transition of the PEC domains from disordered sphere to lamellar morphology (red shaded region in Fig. 6C).

Overall, it can be surmised that the PEC networks are compatible with and resilient towards the inclusion of different types of precursors – with distinct molecular structures, crosslinking mechanisms, functional groups, and polymer origins – and their corresponding covalent networks.

Design guidelines for PEC/covalent IPN hydrogels

This work provides a design paradigm to improve the properties of photocrosslinked hydrogels, pre- and post-crosslinking, by employing PEC hydrogels, composed of oppositely charged block polyelectrolytes, as functional scaffoldings. Here, we have demonstrated the fabrication of

 This journal is © The Royal Society of Chemistry and IChemE 2023

Published on 05 January 2023. Downloaded by University of California - Los Angeles on 5/25/2023 8:37:38 AM.

PEC + precursor hydrogels and PEC/covalent IPN hydrogels with four kinds of photocrosslinkable precursors (PEGA, 4-arm PEGA, GelMA, and AAm), demonstrating the suitability of PEC hydrogels as a scaffolding for photocrosslinkable hydrogels. No modification of the precursors was required to make them compatible with the bPEs, and the four types of PEC + precursor hydrogels and the corresponding IPN hydrogels all featured improvements in their material properties while retaining the PEC microstructure. These improvements are surmised in the schematic shown in Fig. 7.

We note that the extent of improvements in the shear properties of the PEC + precursor hydrogels and of the shear and the tensile properties of the IPN hydrogels depend on the chemical nature and the size of the precursor molecules, which in turn is posited to influence the extent of bridging in the PEC network and the completeness of the covalent network. Thus, the shear and tensile properties of the photocrosslinked IPN hydrogels can be tuned by varying the concentration and sizes of the bPEs and the precursor molecules. Moreover, precursors carrying ionizable functional groups (*e.g.*, GelMA) can interact with the bPE chains, resulting in further improvements of the shear and tensile properties of the IPN hydrogels.

Systematic tuning of the shear properties of the precursors by dispersing them in PEC hydrogels prior to photocrosslinking, creating PEC + precursor hydrogels, enables their application and curing in aqueous environments.[64] Increasing the bPE concentration leads to higher shear moduli, while increasing the precursor concentration leads to a reduction of the shear moduli. The extent of the latter, however, is dependent on the chemical nature and size of the precursor molecules. A small molecular precursor (*e.g.*, AAm) was shown to have negligible influence on the shear moduli, while a large molecule (*e.g.*, PEGDA with 20 000 g mol^{-1}) lowered the shear moduli of PEC + precursor hydrogels notably. Additionally, the reversible and recoverable nature of the self-assembled PEC network imparted strong shear-thinning and quick recovery upon cessation of shear, enabling facile injectability and fast recovery upon deposition of the PEC + precursor hydrogels.[58,62] The improved viscosity and shear properties of the photocrosslinkable precursors can improve their utility in extrusion-based 3D bioprinting, wherein enhancement of inter-layer bonding, prevention of secondary flow, and mitigation of the need for photocrosslinking after deposition of each layer can offer improved printing resolution and enable the construction of intricate architectures. Similarly, the PEC + precursors hydrogels can be molded to conform to an irregular substrate (wound site) and prevent secondary flow at target sites, improving the functionality of existing photocrosslinkable bioadhesives.

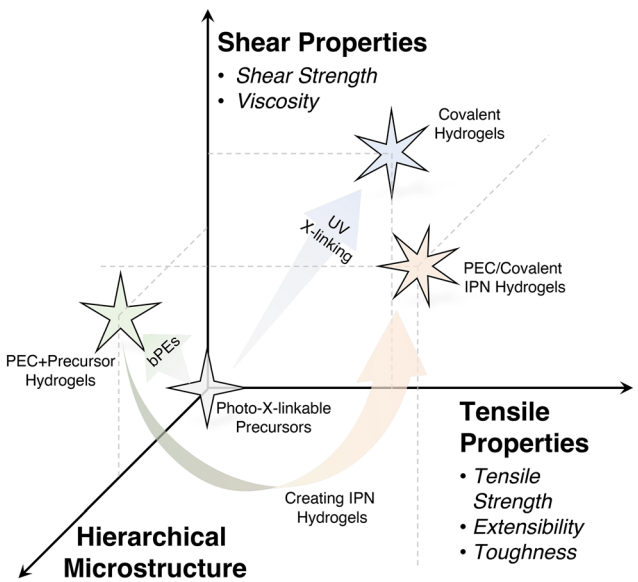

Fig. 7 Design guidelines for PEC-based hydrogels. Photocrosslinking imbues both shear and tensile properties to covalent hydrogels, but no microstructure. Combining of bPEs with precursors introduce microstructural diversity, stronger shear strength, and higher viscosity to the precursor solutions. Upon photocrosslinking, the IPN hydrogels acquire improvements in both tensile and shear properties owing to formation of interpenetrating covalent and PEC networks.

The improvements in the shear properties of the PEC + precursor hydrogels translate into enhanced shear and tensile performance of the IPN hydrogels fabricated by photoirradiation of the PEC + precursor hydrogels. The interpenetration of the PEC and covalent networks reinforces the shear and tensile properties of the resulting IPN hydrogels while preserving the PEC network microstructure (Fig. 7). We note that while the mixing of the bPEs with the photocrosslinkable precursors can reduce the transparency of the PEC + precursor hydrogels as compared to the precursor solutions, the optical density of the PEC + precursor hydrogels was tuneable by regulating bPEs concentration (Fig. S28†). Moreover, the lowered transparency wasn't found to influence the photocrosslinking of the precursors noticeably, as ascertained from the performance of the IPN hydrogels under shear or tensile loads.

In IPN hydrogels, both the shear and the tensile performance can be modulated by varying the bPE or precursor contents. Higher bPE or precursor concentration strengthens the shear moduli of the IPN hydrogels, ascribable to higher crosslink density in the PEC or the covalent network, respectively. The shear moduli of the IPN hydrogels were found to be higher than the linear combination of the moduli of the two networks, highlighting the synergistic contribution of the additional entanglements between the interpenetrated PEC and covalent networks to the shear performance of the IPN hydrogels. At the same time, the reversible assembly of the PEC domains comprising the PEC network contributes to an additional mechanism for stress-dissipation in the IPN hydrogels. Hence, in cases wherein the covalent network formation was not inhibited significantly (*e.g.*, PEC/AAm IPN hydrogels), the tensile strength of the IPN hydrogels improved notably. In contrast, IPN gels wherein the covalent network formation was

Published on 05 January 2023. Downloaded by University of California - Los Angeles on 5/25/2023 8:37:38 AM.

partially inhibited (*e.g.*, PEC/PEGDA and PEC/4-arm PEGA IPN hydrogels) benefitted from improvements in extensibility while the loss of tensile strength from the incomplete covalent network formation were compensated by the enhancements in strength from the PEC network and the additional entanglements between the PEC and the covalent networks. In all cases, the hydrogel toughness improved.

The self-assembled PEC domains constituting the PEC network contribute to additional attributes beyond providing mechanical reinforcement in PEC + precursor hydrogels and IPN hydrogels by serving as reversible physical multi-linkages that aid in energy dissipation and enhancing the bulk strength and toughness. The PEC domains provide a richer microstructural diversity to the IPN hydrogels and also can serve as repositories for controlled encapsulation and release of charged macromolecules (drugs, growth factors)[63] to enable photocrosslinked hydrogels with therapeutic attributes.

Author contributions

S. S. conceptualized the work. D. L. designed and conducted the experiments and analyzed the data. M. G. synthesized Gelatin methacryloyl and assisted D. L. in the synthesis of poly(ethylene glycol) diacrylate. N. A. supervised M. G.'s contributions. D. L. and S. S. wrote the manuscript. S. S. supervised all aspects of the research.

Conflicts of interest

There are no conflicts to declare.

Acknowledgements

This research was supported by National Science Foundation under Grant No. DMR-2048285. This research used the facility of the Advanced Photon Source, a U.S. Department of Energy (DOE) Office of Science User Facility operated for the DOE Office of Science by Argonne National Laboratory under Contract No. DE-AC02-06CH11357. S. S. acknowledges helpful discussion with Prof. Vivek Sharma.

Notes and references

1 J. Yang, R. Bai, B. Chen and Z. Suo, *Adv. Funct. Mater.*, 2020, **30**, 1901693.
2 M. Mehdizadeh and J. Yang, *Macromol. Biosci.*, 2013, **13**, 271–288.
3 N. Annabi, K. Yue, A. Tamayol and A. Khademhosseini, *Eur. J. Pharm. Biopharm.*, 2015, **95**, 27–39.
4 O. Jeon, J. E. Samorezov and E. Alsberg, *Acta Biomater.*, 2014, **10**, 47–55.
5 E. S. Sani, A. Kheirkhah, D. Rana, Z. Sun, W. Foulsham, A. Sheikhi, A. Khademhosseini, R. Dana and N. Annabi, *Sci. Adv.*, 2019, **5**, eaav1281.
6 A. Bal-Ozturk, B. Cecen, M. Avci-Adali, S. N. Topkaya, E. Alarcin, G. Yasayan, Y.-C. E. Li, B. Bulkurcuoglu, A. Akpek and H. Avci, *Nano Today*, 2021, **36**, 101049.
7 Q. Mei, J. Rao, H. P. Bei, Y. Liu and X. Zhao, *Int. J. Bioprint.*, 2021, **7**, 367.
8 I. Pepelanova, K. Kruppa, T. Scheper and A. Lavrentieva, *Bioengineering*, 2018, **5**, 55.
9 L. Ouyang, C. B. Highley, W. Sun and J. A. Burdick, *Adv. Mater.*, 2017, **29**, 1604983.
10 Ž. P. Kačarević, P. M. Rider, S. Alkildani, S. Retnasingh, R. Smeets, O. Jung, Z. Ivanišević and M. Barbeck, *Materials*, 2018, **11**, 2199.
11 M. Sarker, S. Naghieh, N. Sharma and X. Chen, *J. Pharm. Anal.*, 2018, **8**, 277–296.
12 J. H. Galarraga, M. Y. Kwon and J. A. Burdick, *Sci. Rep.*, 2019, **9**, 1–12.
13 S. Derakhshanfar, R. Mbeleck, K. Xu, X. Zhang, W. Zhong and M. Xing, *Bioact. Mater.*, 2018, **3**, 144–156.
14 R. L. Alexa, H. Iovu, J. Ghitman, A. Serafim, C. Stavarache, M.-M. Marin and R. Ianchis, *Polymers*, 2021, **13**, 727.
15 T. Jungst, W. Smolan, K. Schacht, T. Scheibel and J. Groll, *Chem. Rev.*, 2016, **116**, 1496–1539.
16 R. F. Pereira and P. J. Bártolo, *J. Appl. Polym. Sci.*, 2015, **132**, 42458.
17 M. L. Bedell, A. M. Navara, Y. Du, S. Zhang and A. G. Mikos, *Chem. Rev.*, 2020, **120**, 10744–10792.
18 S. Knowlton, B. Yenilmez, S. Anand and S. Tasoglu, *Bioprinting*, 2017, **5**, 10–18.
19 A. GhavamiNejad, N. Ashammakhi, X. Y. Wu and A. Khademhosseini, *Small*, 2020, **16**, 2002931.
20 N. Ashammakhi, S. Ahadian, C. Xu, H. Montazerian, H. Ko, R. Nasiri, N. Barros and A. Khademhosseini, *Mater. Today Bio*, 2019, **1**, 100008.
21 S. Aubert, M. Bezagu, A. C. Spivey and S. Arseniyadis, *Nat. Rev. Chem.*, 2019, **3**, 706–722.
22 Y. Wang, S. Zhang and J. Wang, *Chin. Chem. Lett.*, 2021, **32**, 1603–1614.
23 J. Elisseeff, K. Anseth, D. Sims, W. McIntosh, M. Randolph and R. Langer, *Proc. Natl. Acad. Sci. U. S. A.*, 1999, **96**, 3104–3107.
24 N. Bhattarai, J. Gunn and M. Zhang, *Adv. Drug Delivery Rev.*, 2010, **62**, 83–99.
25 R. Dimatteo, N. J. Darling and T. Segura, *Adv. Drug Delivery Rev.*, 2018, **127**, 167–184.
26 P. Matricardi, C. Di Meo, T. Coviello, W. E. Hennink and F. Alhaique, *Adv. Drug Delivery Rev.*, 2013, **65**, 1172–1187.
27 F. Rizzo and N. S. Kehr, *Adv. Healthcare Mater.*, 2021, **10**, 2001341.
28 M. K. Schesny, M. Monaghan, A. H. Bindermann, D. Freund, M. Seifert, J. A. Eble, S. Vogel, M. P. Gawaz, S. Hinderer and K. Schenke-Layland, *Biomaterials*, 2014, **35**, 7180–7187.
29 E. A. Clark, M. R. Alexander, D. J. Irvine, C. J. Roberts, M. J. Wallace, S. Sharpe, J. Yoo, R. J. Hague, C. J. Tuck and R. D. Wildman, *Int. J. Pharm.*, 2017, **529**, 523–530.
30 W. S. Lim, K. Chen, T. W. Chong, G. M. Xiong, W. R. Birch, J. Pan, B. H. Lee, P. S. Er, A. V. Salvekar and S. S. Venkatraman, *Biomaterials*, 2018, **165**, 25–38.
31 S. Liu, D. C. Yeo, C. Wiraja, H. L. Tey, M. Mrksich and C. Xu, *Bioeng. Transl. Med.*, 2017, **2**, 258–267.

 This journal is © The Royal Society of Chemistry and IChemE 2023

Published on 05 January 2023. Downloaded by University of California - Los Angeles on 5/25/2023 8:37:38 AM.

32 D. Aycan and N. Alemdar, *Carbohydr. Polym.*, 2018, **184**, 401–407.
33 K. Modaresifar, A. Hadjizadeh and H. Niknejad, *Artif. Cells, Nanomed., Biotechnol.*, 2018, **46**, 1799–1808.
34 C. Qi, J. Liu, Y. Jin, L. Xu, G. Wang, Z. Wang and L. Wang, *Biomaterials*, 2018, **163**, 89–104.
35 B. J. Klotz, D. Gawlitta, A. J. Rosenberg, J. Malda and F. P. Melchels, *Trends Biotechnol.*, 2016, **34**, 394–407.
36 Y. Wang, L. H. Koole, C. Gao, D. Yang, L. Yang, C. Zhang and H. Li, *npj Regener. Med.*, 2021, **6**, 1–14.
37 M. Sun, X. Sun, Z. Wang, S. Guo, G. Yu and H. Yang, *Polymer*, 2018, **10**, 1290.
38 H. Tan and K. G. Marra, *Materials*, 2010, **3**, 1746–1767.
39 Q. T. Nguyen, Y. Hwang, A. C. Chen, S. Varghese and R. L. Sah, *Biomaterials*, 2012, **33**, 6682–6690.
40 P. A. Levett, F. P. Melchels, K. Schrobback, D. W. Hutmacher, J. Malda and T. J. Klein, *Acta Biomater.*, 2014, **10**, 214–223.
41 C. Meinert, K. Schrobback, D. W. Hutmacher and T. J. Klein, *Sci. Rep.*, 2017, **7**, 1–14.
42 G. C. Brown, K. S. Lim, B. L. Farrugia, G. J. Hooper and T. B. Woodfield, *Macromol. Biosci.*, 2017, **17**, 1700158.
43 V. H. Mouser, F. P. Melchels, J. Visser, W. J. Dhert, D. Gawlitta and J. Malda, *Biofabrication*, 2016, **8**, 035003.
44 L. Bian, M. Guvendiren, R. L. Mauck and J. A. Burdick, *Proc. Natl. Acad. Sci. U. S. A.*, 2013, **110**, 10117–10122.
45 J. W. Hayami, S. D. Waldman and B. G. Amsden, *Macromol. Biosci.*, 2016, **16**, 1083–1095.
46 S. J. Buwalda, K. W. M. Boere, P. J. Dijkstra, J. Feijen, T. Vermonden and W. E. Hennink, *J. Controlled Release*, 2014, **190**, 254–273.
47 J. R. Choi, K. W. Yong, J. Y. Choi and A. C. Cowie, *BioTechniques*, 2019, **66**, 40–53.
48 Y. Hua, H. Xia, L. Jia, J. Zhao, D. Zhao, X. Yan, Y. Zhang, S. Tang, G. Zhou and L. Zhu, *Sci. Adv.*, 2021, **7**, eabg0628.
49 T. Thakur, J. R. Xavier, L. Cross, M. K. Jaiswal, E. Mondragon, R. Kaunas and A. K. Gaharwar, *J. Biomed. Mater. Res., Part A*, 2016, **104**, 879–888.
50 S. Bian, Z. Zheng, Y. Liu, C. Ruan, H. Pan and X. Zhao, *J. Mater. Chem. B*, 2019, **7**, 6488–6499.
51 J. M. Townsend, E. C. Beck, S. H. Gehrke, C. J. Berkland and M. S. Detamore, *Prog. Polym. Sci.*, 2019, **91**, 126–140.
52 C. Creton, *Macromolecules*, 2017, **50**, 8297–8316.
53 E. Khare, N. Holten-Andersen and M. J. Buehler, *Nat. Rev. Mater.*, 2021, **6**, 421–436.
54 X. Lin, X. Wang, L. Zeng, Z. L. Wu, H. Guo and D. Hourdet, *Chem. Mater.*, 2021, **33**, 7633–7656.
55 J. Cao, J. Li, Y. Chen, L. Zhang and J. Zhou, *Adv. Funct. Mater.*, 2018, **28**, 1800739.
56 Z.-J. Meng, J. Liu, Z. Yu, H. Zhou, X. Deng, C. Abell and O. A. Scherman, *ACS Appl. Mater. Interfaces*, 2020, **12**, 17929–17935.
57 Y. S. Zhang and A. Khademhosseini, *Science*, 2017, **356**, eaaf3627.
58 J. N. Hunt, K. E. Feldman, N. A. Lynd, J. Deek, L. M. Campos, J. M. Spruell, B. M. Hernandez, E. J. Kramer and C. J. Hawker, *Adv. Mater.*, 2011, **23**, 2327–2331.
59 E. A. Appel, J. del Barrio, X. J. Loh and O. A. Scherman, *Chem. Soc. Rev.*, 2012, **41**, 6195–6214.
60 H. Fan and J. P. Gong, *Macromolecules*, 2020, **53**, 2769–2782.
61 W. Hu, Z. Wang, Y. Xiao, S. Zhang and J. Wang, *Biomater. Sci.*, 2019, **7**, 843–855.
62 S. Srivastava, M. Andreev, A. E. Levi, D. J. Goldfeld, J. Mao, W. T. Heller, V. M. Prabhu, J. J. de Pablo and M. V. Tirrell, *Nat. Commun.*, 2017, **8**, 14131.
63 S. Srivastava, A. E. Levi, D. J. Goldfeld and M. V. Tirrell, *Macromolecules*, 2020, **53**, 5763–5774.
64 D. F. Li, T. Gockler, U. Schepers and S. Srivastava, *Macromolecules*, 2022, **55**, 4481–4491.
65 A. Mostafavi, M. Samandari, M. Karvar, M. Ghovvati, Y. Endo, I. Sinha, N. Annabi and A. Tamayol, *Appl. Phys. Rev.*, 2021, **8**, 041415.
66 M. Ghovvati, S. Baghdasarian, A. Baidya, J. Dhal and N. Annabi, *J. Biomed. Mater. Res., Part B*, 2022, **110**, 1511–1522.
67 G. M. Cruise, D. S. Scharp and J. A. Hubbell, *Biomaterials*, 1998, **19**, 1287–1294.
68 J. Van der Gucht, E. Spruijt, M. Lemmers and M. A. C. Stuart, *J. Colloid Interface Sci.*, 2011, **361**, 407–422.
69 S. Srivastava and M. V. Tirrell, *Adv. Chem. Phys.*, 2016, **161**, 499–544.
70 C. E. Sing and S. L. Perry, *Soft Matter*, 2020, **16**, 2885–2914.
71 M. Kirsch, L. Birnstein, I. Pepelanova, W. Handke, J. Rach, A. Seltsam, T. Scheper and A. Lavrentieva, *Bioengineering*, 2019, **6**, 76.
72 M. Zhu, Y. Wang, G. Ferracci, J. Zheng, N.-J. Cho and B. H. Lee, *Sci. Rep.*, 2019, **9**, 1–13.